Coverage Dependent Rate-Driving Force Relationships: Hydrogen Transfer from Cerium Oxide Nanoparticle Colloids

Rishi G. Agarwal and James M. Mayer*

Department of Chemistry, Yale University, New Haven, CT 06520-8107, USA

Keywords

Abstract. Rate-driving force relationships, known as Brønsted-Evans Polanyi (BEP) relations, are central to many methods for predicting the performance of heterogeneous catalysts and electrocatalysts. Methods such as Tafel plots and 'volcano' analyses often assume the effect of adsorbate coverage on reaction rate across different materials is constant and known. Here we use UV-visible spectroscopy to test these assumptions, by measuring rates of net hydrogen atom transfer from colloidal cerium oxide nanoparticles (nanoceria) to organic reagents at varying surface CeO–H bond strengths and surface coverages. The resulting rate constants follow a linear BEP relationship, $\Delta\log(k) = \alpha\Delta\log(K_{eq})$, across two sizes of nanoceria, two organic reagents, and a ~10 kcal mol^{-1} range of CeO–H bond strengths. Interestingly, the Brønsted slope is only 0.2, demonstrating that the rate constants are far less insensitive to CeO–H bond strength, than would commonly be assumed for a heterogeneous nanomaterial. Furthermore, we observe a Brønsted slope >1 when altering the reaction driving force via the organic reagent bond strength instead of that of CeO–H. The implications of these Brønsted slopes for either concerted or stepwise mechanisms are discussed. To our knowledge, these are the first solution-phase measurements of BEP relationships for hydrogen coverage on a (nano)material.

Introduction

Use of a thermochemical property as a descriptor for the relative kinetic properties of a set of reactions is common throughout chemistry. In 'volcano plots' or similar analyses, the same reaction is compared on different surfaces by plotting the computed $\Delta G°$ of a single reaction step against an experimental metric of kinetic prowess, such as exchange current density or reaction rate.[1-4] These analyses have proven powerful in the search for new heterogeneous (electro)catalysts for fuel-forming processes,[5-7] where the relevant $\Delta G°$ is often the free energy of hydrogen adsorption ($\Delta G°_H$) at an interface.[4] While this approach has been questioned,[2,8,9] and significant work has been done to circumvent the theoretical limits of catalyst rate and efficiency that it implies,[10-12] its general tenants have been broadly influential.

One key theoretical basis for such analyses is the longstanding empirical Brønsted-Evans Polanyi (BEP) linear relationships between the free energy of activation and free energy of the reaction, or equivalently, between the logarithms of the rate and equilibrium constants (eqs 1a and b; $\Delta\ln(k) \propto \Delta\Delta G^‡$ and $\Delta\ln(K_{eq}) \propto \Delta\Delta G°$).[5,13-17] These two equations have the same proportionality constant, the Brønsted α, which is typically between 0 and 1.[18-22] The values of α can in some cases be related to the position of the transition state along the reaction coordinate, with 1 being closest to products.[18-22]

$$\Delta G^‡ = \alpha\Delta G° + c \quad (1a)$$

$$\log(k) = \alpha\log(K_{eq}) + d \quad (1b)$$

The BEP relation was developed for a single elementary reaction step in homogeneous media (gas or solution), with the $\Delta G^‡$ and $\Delta G°$ referring specifically to that one step.[23,24] However, similar relationships, also denoted as BEP relations, are often applied to surfaces, and other systems where the mechanism is not completely known. The application of BEP models to multistep catalytic reactions on different materials surfaces is common but often requires that the energies of different intermediates and transition states linearly correlate with each other and with the descriptor, and that the Brønsted α's do not vary substantially from one reaction to another.[4,6,25] It is this use of linear correlations, well supported by computational studies,[5,26,27] that gave rise to the term 'scaling relationships' to describe this approach. A number of more detailed models are also being developed, such as those with microkinetic modeling and methodologies such as the Degree of Rate Control.[8,28-32]

Another key assumption in the common use of BEP relations for surface reactions is that the dependence of the thermodynamic and kinetic parameters on *surface coverage* is known and constant across different materials. Analyses of solution and gas phase reactions can assume *a priori* that all the molecules are the same over a wide range of concentration or partial pressure (though there are non-idealities at high concentrations or pressures). On a surface, however, there are often interactions among adsorbates that shift the adsorbate properties as a function of coverage.[33-36] The effect of adsorbate interactions on BEP analyses has received considerably less consideration, and coverage effects are not generally considered in big picture 'volcano plot' analyses. However, they can be quite significant. For underpotential deposited hydrogen (H_{upd}) on Pt(111) single crystal surfaces, a model electrochemical adsorption process, the adsorption energy varies with Pt–H coverage

over a range of 0.5 eV or 12 kcal mol^{-1}.[37] While H_{upd} is not the active species in the hydrogen evolution reaction (HER), its range of adsorbate energies is nearly half the width of the 'volcano plot' for the HER,[38] or roughly six-times greater than the 2 kcal mol^{-1} range expected for a Langmuirian, surface adsorption process.[39] While calculated and experimental measures of the coverage dependance of hydrogen adsorption are possible for well-defined surfaces such as Pt(111),[40] similar reports for ill-defined catalytic surfaces – especially those of binary materials – generally do not exist.[41-43] The heterogeneity of these surfaces has limited the number of experimental studies which have probed the effect of coverage on the *kinetics* of hydrogen transfer from (nano)materials.[37,44]

Here we take advantage of our previous measurements of CeO–H bond dissociation free energies (BDFEs) for oleate-capped cerium oxide nanoparticle colloids (OLE-Ce) in tetrahydrofuran (THF) solutions.[45] That study analyzed equilibria between OLE-Ce and organic molecules that involved the exchange of H-atoms between the two, where addition of each H to OLE-Ce formed one surface OH group with reduction of one Ce^{4+} to Ce^{3+}. This reaction can be viewed as a net hydrogen atom transfer (HAT), or a proton-coupled electron transfer (PCET) in which protonation of an oxide is coupled to reduction of a Ce^{4+}. This stoichiometry implies that changes in the number of Ce^{3+} ions correspond to the changes in the surface coverage of "active" H. This study deals only with the active surface H that can be transferred as a hydrogen atom to a molecular abstractor. There are likely other, spectator OH groups on the surface that are not reactive in this way, because they lack a coupled Ce^{3+} ion nearby; these are not considered in the surface coverage discussed here. The dramatic difference between these two classes of surface H was recently demonstrated in a computational study of TiO2 slabs with surface H.[46] In our previous study, the BDFEs of the active CeO–H bonds were shown to vary substantially with the average redox state (%Ce^{3+}) of OLE-Ce. The wide range of BDFEs, over 13 kcal mol^{-1}, had not previously been shown for cerium oxide. We expect that the phenomenon will prove common to many binary materials.[45,47]

The current study reports unique measurements of the rates of net hydrogen atom, or equivalently proton-coupled electron transfer (e^-/H^+, PCET), from O–H groups at the surface of nanoceria. The variation of these rates as a function of hydrogen coverage and hydrogen adsorption free energy are described. To simplify the system as much as possible, the studies reported below probe the net transfer of a hydrogen atom from OLE-Ce to 2,2-diphenyl-1-picrylhydrazyl radicals (DPPH) via UV-Vis spectroscopy (Scheme 1). DPPH and its more sterically encumbered analog 2,2-di(4-*tert*-octylphenyl)-1-picrylhydrazyl (DPPHL [L for large]) were chosen because of their solution-phase stability and large optical extinction coefficients.

Scheme 1. Net Hydrogen Atom Transfer from OLE-Ce to Substituted Picrylhydrazyls

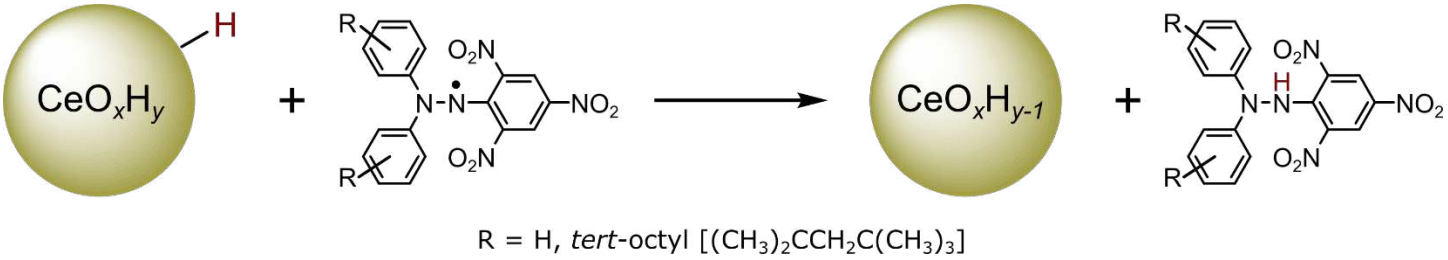

The data presented below demonstrate that the log of the rate constant for net hydrogen atom transfer from nanoceria to DPPH and DPPHL varies linearly with the CeO–H BDFE, or hydrogen adsorption free energy, but only weakly. The slope of this relationship, the Brønsted α, is only 0.2 over a 10 kcal mol^{-1} range of driving forces. Additionally, a separate relationship between the rate constant and the BDFE of the reduced organic reagent is measured to be >1. The discrepancies between these two slopes may originate from a multi-step reaction mechanism, or an imbalanced transfer of e^- and H^+ in a single-step reaction, as has been discussed in molecular systems.[48-51] The mechanistic evidence for these competing hypotheses is presented along with their broader implications for the use of BEP relationships in catalytic models. This study is potentially important for understanding why cerium oxide is so effective as a catalyst support.[42,52] Furthermore, these are, to the best of our knowledge, the first solution-phase experimental measures of coverage-dependent BEP relationships for hydrogen transfer from a material, nanoscale or otherwise.

Experimental

Oleate-capped cerium oxide nanoparticles (OLE-Ce) were prepared following a previously reported procedure.[45] Briefly, nanoparticles were precipitated through base hydrolysis of a cerium oleate complex formed from ceric ammonium nitrate and sodium oleate. After multiple washing and drying steps, nanoparticles were stored in an N_2-filled glovebox as a colloid in tetrahydrofuran (THF) at −30 °C.

Reaction kinetics were followed by monitoring the decay of an organic oxidant (usually DPPH) by UV-visible (UV-vis) absorption spectroscopy. Kinetics were always performed with a significant excess of hydrogen equivalents (on OLE-Ce) as compared to the organic oxidant. Reactions were initiated by adding OLE-Ce to THF solutions of the organic oxidant in an N_2-filled glovebox. Full experimental details are provided in the Supplementary Information.

Results

I. Kinetics of nanoceria oxidation.

This study used oleate-capped cerium oxide nanoparticles (OLE-Ce) reduced to varying extents to determine how the hydrogen adsorption free energy of OLE-Ce affects the rate of hydrogen atom transfer to a well-defined organic oxidant, Scheme 1. Studies were performed in tetrahydrofuran (THF) with two batches of OLE-Ce. By transmission electron microscopy (TEM), one batch contained nanoparticles with an

average diameter of 1.8 ± 0.2 nm (**Ce-1**) and the other had larger nanoparticles (**Ce-L**, d = 4.0 ± 0.4). Further details on the characterization of these nanoceria colloids are provided in our previous work.[45] OLE-Ce colloids were first reduced by adding varying amounts of 1,8-dichloro-9,10-dihydroxyanthracene, a strong PCET reductant (H_2DCAQ, $BDFE_{avg}$ = 55.4 kcal mol^{-1} in THF).[45,53] Quantitative donation of two hydrogen atoms from H_2DCAQ to OLE-Ce, confirmed by ^{1}H NMR quantification of the 1,8-dichloro-9,10-anthraquinone (DCAQ) product, enables precise control over the average redox state, or %Ce^{3+}, of OLE-Ce. The partially reduced OLE-Ce were then reacted with a small amount of DPPH, and the decay of the purple DPPH over seconds to minutes was evident to the eye as the reactions changed to orange.

The rates of DPPH decay in the presence of reduced stock solutions of either **Ce-1** or **Ce-L** were monitored by UV-Vis at the DPPH absorbance maximum, 519 nm (Figure S1). At this wavelength, and under the conditions used in this study, the primary contribution to the absorbance spectrum is DPPH before the reaction, and DPPH-H after completion (Figure 1A). Formation of the 1e^-/1H^+ reduced product—1,1-diphenyl-2-picrylhydrazine (DPPH-H)—in these reactions was confirmed previously by ^{1}H NMR.[45] Concentrations were chosen so that there were minimal changes in the %Ce^{3+}—and therefore the CeO–H bond strength and surface H coverage—over the course of the reaction. This required a significant excess of hydrogen equivalents (H's bound to OLE-Ce) as compared to DPPH. In many cases, the rate data were analyzed both by exponential fits and by the method of initial rates, which further insured that the changes in %Ce^{3+} were small over the region analyzed. With this experimental design, the measured kinetics can be connected to a well-defined reaction driving force: the difference in the BDFEs of the ceria and the DPPH.

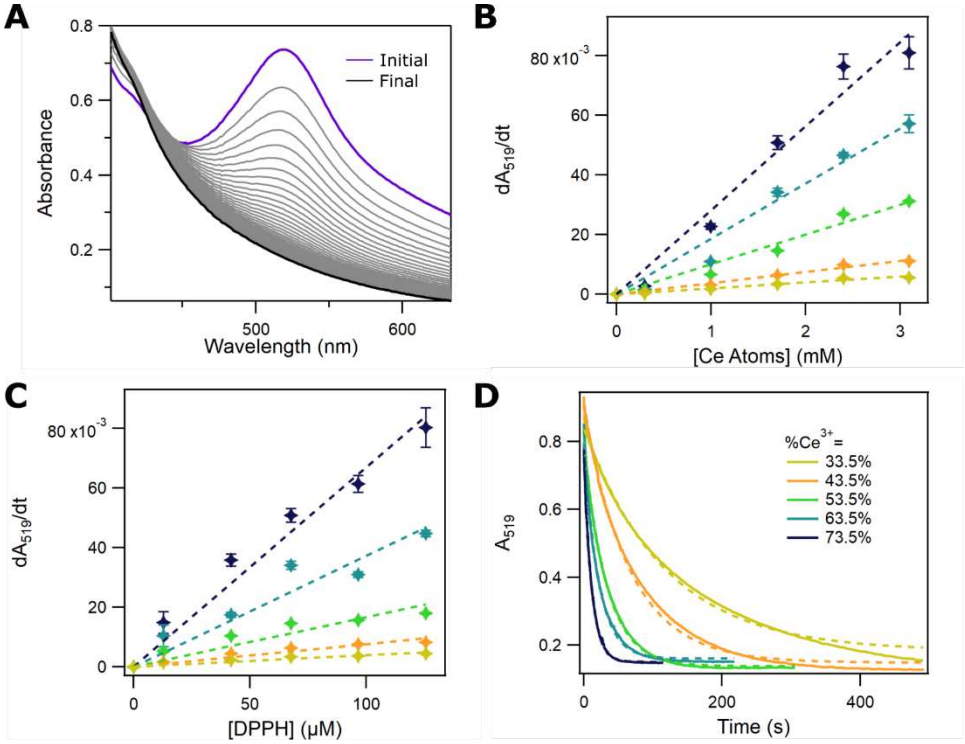

Figure 1. Full spectrum and single-wavelength kinetics of the reaction between reduced **Ce-1** and DPPH. Denoted concentrations are for sample after mixing, but before reaction initiation. (**A**) Full spectrum kinetics collected by stopped-flow UV-vis measurements. Solution contained [DPPH] = 67 μM and [Ce atoms] = 4.4 mM at %Ce^{3+} = 69%. The reaction took ~30 seconds to complete. (**B**) Initial rates kinetic dependence of DPPH decay on the concentration of Ce atoms at five different %Ce^{3+} levels in **Ce-1** nanoparticles (legend in part D). [DPPH] = 68 μM for all samples. (**C**) Initial rates kinetic dependence of DPPH decay on [DPPH] at varying %Ce^{3+} for **Ce-1**. [Ce atoms] = 1.7 mM for all samples. For (B) and (C) dashed lines are linear fits with the y-intercept set as zero and data is colored coded per the legend in (D). (**D**) Full single wavelength kinetic traces of DPPH decay at varying %Ce^{3+} for **Ce-1** where [Ce atoms] = 3.1 mM and [DPPH] = 68 μM for all samples. Dashed lines are single exponential fits.

Analysis of the kinetic data by the method of initial rates involved taking linear fits of single wavelength kinetics over the segment from 5-15% of total reaction progress. Analyses of the 0-10% section gave similar results, but with larger error bars for several concentrations (Figure S3). The greatest change in %Ce^{3+} for **Ce-1** in a run analyzed by the method of initial rates was 2.3%, which would correspond to a change in the reaction free energy of 0.4 kcal mol^{-1} for **Ce-1** nanoparticles (see below). Dependences on the concentrations of Ce atoms and DPPH are both first order across a range of %Ce^{3+} values for **Ce-1** (Figure 1B and 1C) and for **Ce-L** (Figure S4). The reactions therefore follow a simple bimolecular rate law under these conditions (eq 2). Each rate constant (k) was determined from the slope of the DPPH concentration dependence and also from the slope of the dependence on total concentration of Ce atoms in solution ([Ce atoms]). Samples with the highest ratio of reduced Ce atom (or hydrogen atom) equivalents to DPPH were also fit to exponentials as an alternative method for determining k (Figure 1D). The change in **Ce-1** %Ce^{3+} is 2.2% for the reaction to go to completion in these samples. For the kinetic studies of **Ce-1** colloids these three ways of determining the reaction rate constant agree well, with a standard deviation of roughly ±25%, thereby demonstrating that each method of analysis is consistent with the second order rate law (eq 2).

$$\text{rate} = k[\text{DPPH}][\text{Ce atoms}] \quad (2)$$

II. Kinetic-thermodynamic correlations.

The driving force ($\Delta G°$) for these reactions is the difference between the BDFE of the OLE-Ce colloid ($BDFE_{Ce}$) and that of DPPH-H. In order to determine $BDFE_{Ce}$, the relevant regions of previously reported relationships between $\%Ce^{3+}$ and BDFE for **Ce-1** and **Ce-L** were fit using linear regressions. These lines of best fit show R^2 values close to 1 and provide a simple method for determining the $BDFE_{Ce}$ for any level of OLE-Ce reduction (Figure S5). Subtraction of the BDFE of DPPH-H (73.5 kcal mol^{-1} in THF)[53] from the relevant $BDFE_{Ce}$ gives $\Delta G°$ for the reaction. In a typical example, a **Ce-1** sample with $\%Ce^{3+}$ = 54% was determined to have $BDFE_{Ce}$ = 60.7 kcal mol^{-1} so the $\Delta G°$ for the reaction was –12.8 ± 0.6 kcal mol^{-1}. Overall, the experiments reported here covered a range of driving forces from –6.8 to –16.6 kcal mol^{-1}, or ln(K_{eq}) values from 11.5 to 28.0 (a range of 10^7 in K_{eq}).

The rate constants were then correlated with the equilibrium constants. Plotting ln(k) versus ln(K_{eq}), *both experimentally determined*, shows a linear correlation for reactions between DPPH and **Ce-1** (Figure 2A). A quite similar line was determined for the analogous reactions of **Ce-L**. This linear relationship is what is predicted by the BEP principle (eq 1b above).

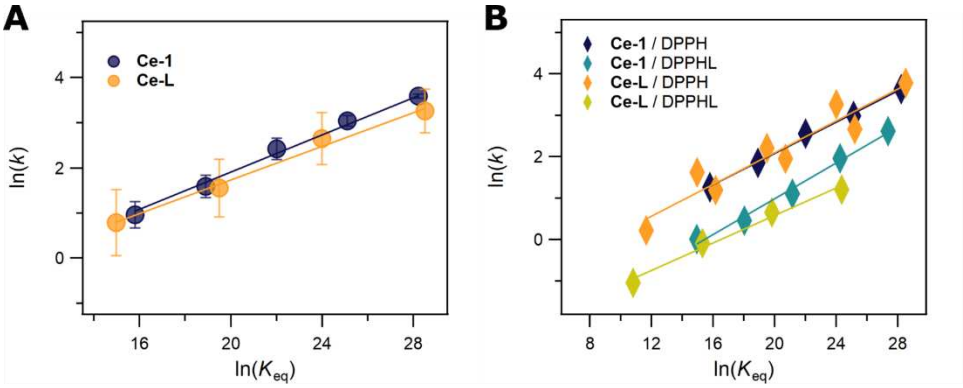

Figure 2. Dependence of reaction rate constant (ln(k)) on driving force (ln(K_{eq})), for reactions of **Ce-1** and **Ce-L** nanoparticles. (**A**) Reactions with DPPH, where values of k are the averages of values derived from the DPPH and Ce atom initial rates dependences using eq 2, as well as from single exponential fits of full trace kinetics. Error bars denote the standard deviation from these three methods of measuring k. (**B**) Relationships are shown for reactions with both DPPH and DPPHL. Here, values of k are derived only from exponential fits of data collected where [DPPH] = 68 μM, [DPPHL] = 79 μM, [Ce atoms] = 3.1 mM for **Ce-1**, and [Ce atoms] = 8.5 mM for **Ce-L**. Uncertainties are smaller than the diamond-shaped data points. For both figures, values of ln(K_{eq}) are determined from $\Delta G° = BDFE_{Ce} - BDFE_{DPPH(L)-H}$. In (A), the slope of the **Ce-1** linear fit is 0.21 ± 0.02 and that for **Ce-L** is 0.19 ± 0.06; the slopes of the linear fits in (B) are given in Table 1.

Similar studies were also performed with 2,2-di(4-*tert*-octylphenyl)-1-picrylhydrazyl (DPPHL [L for large]) in order to probe the kinetic effect of altering reaction driving force via the BDFE of the newly formed N-H bond of the organic PCET oxidant. Using a recently published open-circuit potential method,[53] the BDFE of 1,1-di(4-*tert*-octylphenyl)-2-picrylhydrazine (DPPHL-H) was determined to be 73.0 kcal mol^{-1} in THF; or 0.5 ± 0.2 kcal mol^{-1} less oxidizing than DPPH (Figure S6). Kinetic studies of the reaction between reduced OLE-Ce and DPPHL were followed at absorbance maximum of the radical, 541 nm (Figure S1). As with DPPH, first order dependences on the concentrations of Ce atoms and DPPHL were observed (Figure S7). Therefore, the same bimolecular rate law applies, and comparable k's could be obtained. The results of the DPPHL reactions form BEP relationships very similar to those for DPPH, just shifted down and to the left (Figure 2B). They are shifted left, to lower driving forces, because the DPPHL–H bond is 0.5 kcal mol^{-1} weaker than the DPPH–H bond.

Plots of BEP relationships for all four combinations of **Ce-1** or **Ce-L** with DPPH or DPPHL, ln(k) vs. ln(K_{eq}), are in Figure 2B and the data are in Table 1. These four Brønsted α values are essentially the same within the uncertainties, all 0.20 ± 0.03. This value is lower than the typical α of ½ for single-step reactions that are not too exergonic or endergonic. Since these reactions are only modestly exergonic, $\Delta G°$ between –6.8 and –16.6 kcal mol^{-1}, the α = 0.2 means that the rate constants of these reactions are far less sensitive to the overall reaction driving force than would normally be expected. Specifically, the variation in K_{eq} over a range of 10^7 only causes changes in k by a factor of 25.

The data shown in Figure 2B and slopes, or α's, given in Table 1 are from exponential fits. These fits, as shown in Figure 1C, are not perfect even with large excesses of Ce atoms. To test the validity of the exponential fit analysis, we used a version of Variable Time Normalization Analysis (VTNA).[54] This involves stretching the time axis to overlay the exponential decays at differing values of $\%Ce^{3+}$ (Figure S8). This treatment gives a close overlay of all plots. Furthermore, the "stretch-factors" used to generate the overlaid plots should be a direct measure of the relative rates. Plotting the logarithm of the "stretch-factor" versus the logarithm of the K_{eq} gives a line with a slope of 0.20 ± 0.01, as expected. These analyses confirm that any deviations from the exponential fits do not lead to systematic errors in the reported rate constants which would significantly affect the slopes of the reported BEP relationships.

Table 1. BEP Relationships Slopes [a]

reactants	Slope	Range of ΔG°	Range of ΔG‡
Ce-1 / DPPH	0.19	7.2	1.4
Ce-1 / DPPHL	0.22	7.2	1.5
Ce-L / DPPH	0.19	9.8	2.1
Ce-L / DPPHL	0.17	7.9	1.3

[a] All slopes [Brønsted alphas (α)] are from ln(k) vs ln(K_{eq}) plots where values of k are determined from exponential fits. The uncertainty for all values of α is ± 0.02. Values of $\Delta G°$ and $\Delta G^{‡}$ are in kcal mol^{-1}.

III. Control Experiments and Effects of Additives

In order to gain a clearer picture of the reaction mechanism we tested the effects of various additives on the kinetics. As the reaction formally has a proton transfer component, the effects of acids and bases, as well as ligands were tested. Addition of >3 mM of oleic acid, triphenyl phosphine oxide, or 150 μM of DPPH-H was found to *decrease* the reaction rate by a factor of 2 or more (Figure S9). In contrast, the addition of >25 mM of MeOH or H_2O was shown to *increase* the reaction rate by a factor of 2 or more (Figure S9C). Cerium(III) oleate ($Ce(OLE)_3$), a known species in OLE-Ce stock solutions,[45] had no effect on the rate (Figure S9C). The effect of the concentration of free oleate anions on the kinetics could not be tested due to incompatibilities with DPPH, DPPH-H, and DPPHL-H. Another compound that could potentially be important to the kinetics is DCAQ which is present in ceria stock solutions because of the reductive pretreatment with H_2DCAQ. Addition of large excesses of DCAQ to nanoparticle stocks at a range of $\%Ce^{3+}$ values had no effect on reaction kinetics (Figure S10). While these effects are generally modest compared to the changes in k and K_{eq} (×25 and ×10^7, respectively), these experiments show that changes to the reaction solution modulate the reactivity of OLE-Ce.

The mechanism of this PCET reaction could occur via a stepwise process with a charged intermediate or a concerted process without one. A stepwise path could be by initial electron transfer (ET) followed by proton transfer (PT), or by PT then ET. Increasing the solution ionic strength through the addition of 0 to 5.3 mM sodium tetrakis[3,5-bis(trifluoromethyl)phenyl]borate ($NaBAr^F$) had no discernible effect on the reaction rate (Figure S11). Typically, increasing ionic strength should facilitate reactions with intermediates of higher charge.

The H/D kinetic isotope effect (KIE) was measured. Our previous study concluded that the majority of redox active sites are surface CeO–H groups.[45] To form CeO-D groups, surface hydroxyl groups were exchanged with either dried perdeutero methanol (MeOH-d_4) or deuterium oxide (D_2O). Methanol and MeOH-d_4 were dried over activated 3Å sieves and distilled before use. Exchanges were performed at room temperature through simple addition to the reduced OLE-Ce stock solution a few minutes before dilution with THF, stirring at 1000 rpm, and reaction initiation via the addition of the organic oxidant. Exchanges were also performed by sequentially removing solvent *in vacuo* and adding deuterated solvent. Experiments were performed by comparing reaction kinetics of exchanged OLE-Ce and OLE-Ce treated in the same manner with the *proteo* solvent (CH_3OH or H_2O). All of the kinetic measurements, using both DPPHL and DPPH, gave KIEs of 1 within the uncertainties (1.01 ± 0.04 with DPPHL, 1.03 ± 0.04 for DPPH). The implications of these various experiments are discussed below.

IV. Inter-nanoparticle Hydrogen Exchange

To further understand the kinetic complexity of OLE-Ce H-atom transfer reactivity, it is of interest to understand the timescale of inter-nanoparticle hydrogen exchange. If the rate of this hydrogen exchange is faster than the reaction rate then it will not be seen in kinetics being probed, but if it is slower it could create speciation of the OLE-Ce in solution over the course of the reaction. It is important to note that in the above studies, any effect of hydrogen exchange has been mitigated by performing reactions in a large excess of H-atoms added to DPPH so that the net change in $\%Ce^{3+}$ is small (<2.3%). Therefore, under these conditions, any inter-nanoparticle hydrogen exchange will not significantly affect the distribution of hydrogen coverages. Nevertheless, the timescale of this exchange is, fundamentally, of interest and provides one measure of the self-exchange between nanoparticles in the OLE-Ce colloid.

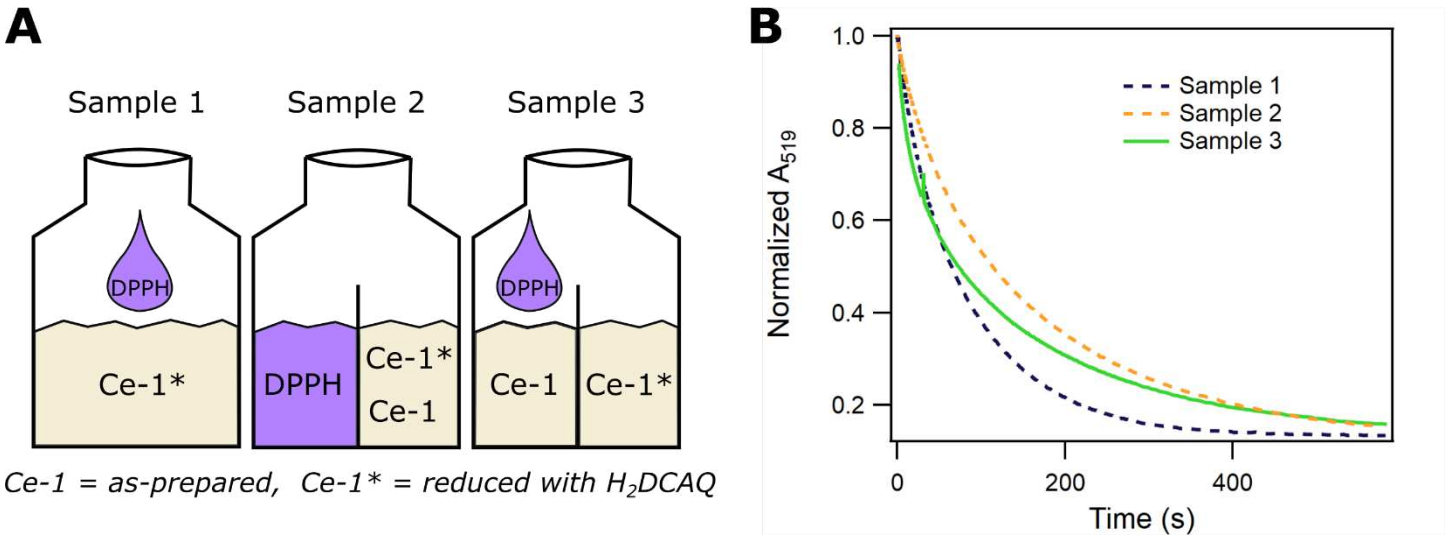

Figure 3. Schematic and results for the study of H-exchange between nanoceria. Three reactions are carried out in quartz cuvettes including those with a quartz divider that extends much of the way up the cell (a tandem-mixing cell). Shaking the tandem-mixing cell mixes the two solutions on the two sides. **(A)** Schematic of the three quartz cuvettes used to carry out the three reactions before the reaction between **Ce-1** reduced by H_2DCAQ (**Ce-1***) and DPPH is initiated. Sample 1 is a standard quartz cuvette, where the reaction was initiated through addition of the **Ce-1*** stock solution as opposed to shaking. Samples 2 and 3 are tandem-mixing cells which only differ by which stock solutions are in each compartment. The total concentration of added hydrogen atom equivalents was 0.37 mM in each sample. **(B)** Kinetic traces for the decay of DPPH absorbance in the three samples. Sample 1 contained [Ce atoms] = 0.93 mM and [DPPH] = 74 μM. Upon mixing, Samples 2 and 3 contained [Ce atoms] = 1.8 mM and [DPPH] = 74 μM.

To test for H-exchange, three reactions were monitored in parallel (Figure 3). Sample 1 contained one equivalent of highly reduced **Ce-1**, indicated as **Ce-1***, Sample 2 contained one equivalent of the same **Ce-1*** plus one equivalent of as-prepared **Ce-1** (23.5% Ce^{3+})[45] with the mixture left to equilibrate overnight, and Sample 3 had contents identical to Sample 2 except that the **Ce-1*** and **Ce-1** were kept separate until the reaction was initiated (Figure 3A). If there were no exchange of H between **Ce-1** nanoparticles, all three reactions would have proceeded similarly to consume the highly reduced **Ce-1**, and only later would the significantly slower oxidation of the as-prepared **Ce-1** occur. In the limit of very fast redox exchange, Sample 1 would react faster than the other two since the average hydrogen loading per **Ce-1** nanoparticle and reaction driving force would have been the highest.

The kinetic traces for Samples 1 and 3 are very similar at short times, indicating that the 1 equivalent of highly reduced **Ce-1** in Sample 3 had not rapidly equilibrated with the more oxidized as-prepared **Ce-1** nanoparticles. However, Sample 2 reacted more slowly at short times, showing that H-exchange did occur between the highly reduced and as-prepared **Ce-1** overnight. After 5-6 minutes, the traces of Samples 2 and 3 became more similar, indicating that the H-exchange is occurring on this timescale (Figure 3B). Comparison with the few studies that have probed the timescale of H-exchange between metal oxide nanoparticles reveals this value is much slower than apparent H-exchange for dodecylamine-capped ZnO nanoparticles in toluene (EPR timescale),[55] and is a bit faster than the rate of roughly isoergic H-transfer between ZnO and TiO_2.[56] These data illustrate a diversity in the intrinsic kinetics of hydrogen transfer across various colloidal metal oxide nanomaterials.

Discussion

I. Normalizing Kinetics for Surface Active Sites

The reaction between a DPPH (or DPPHL) molecule and reduced OLE-Ce colloids involves the net transfer of one hydrogen atom. The measured rate constants depend on the overall driving force for this reaction, but only to a modest extent (Table 1). Across all conditions, the measured $\log(k)/\log(K_{eq})$ slopes—the BEP slopes α — are 0.19 ± 0.02. This includes both **Ce-1** and **Ce-L**, with the latter having a larger estimated uncertainty in α of ±0.06. The comparable lines for **Ce-1** and **Ce-L** effectively overlay in Figure 2. Thus, the slope is not significantly affected by either hydrazyl substitution or nanoparticle size.

The similarity of the **Ce-1** and **Ce-L** reactions is somewhat surprising, given the simplicity of the rate law presented in eq 2. While the rate law was expected to be first order in [Ce atoms], not all cerium atoms are reactive. In our previous report, we demonstrated that the active sites are surface CeO–H groups.[45] Here we use the previously determined ratios of surface to total cerium atoms (R_{surf})[45] to estimate [Ce_{active}] as R_{surf}[Ce atoms]. Making this change in the rate law yields a corrected rate constant, $k_{corr} = k/R_{surf}$ (eq 3).

$$\text{rate} = k_{corr}[\text{DPPH}][Ce_{active}] \quad (3)$$

Application of this surface-site correction *does not change the slope* of any of the BEP relationships, but instead simply shifts the data vertically on the plot by $-\ln(R_{surf})$. Since R_{surf} for **Ce-1** is 0.85 and that for **Ce-L** is 0.39, the data for each are translated by 0.16 and 0.94, respectively.[45] Interestingly, this correction causes the relationships shown for **Ce-1** and **Ce-L** in Figure 2A to separate slightly, so that the kinetics of **Ce-L** reactivity are a little faster than those of **Ce-1** at the same driving force (Figure 4A). This difference is consistent with our previous observation that the thermodynamic hydrogen adsorption isotherms for **Ce-1** and **Ce-L** do not overlay even with this correction.[45] Despite this small difference, the closeness of the lines in Figure 4 indicates that the α = 0.2 is a characteristic of the reaction between OLE-Ce and DPPH(L), independent of the size or nanoparticle batch.

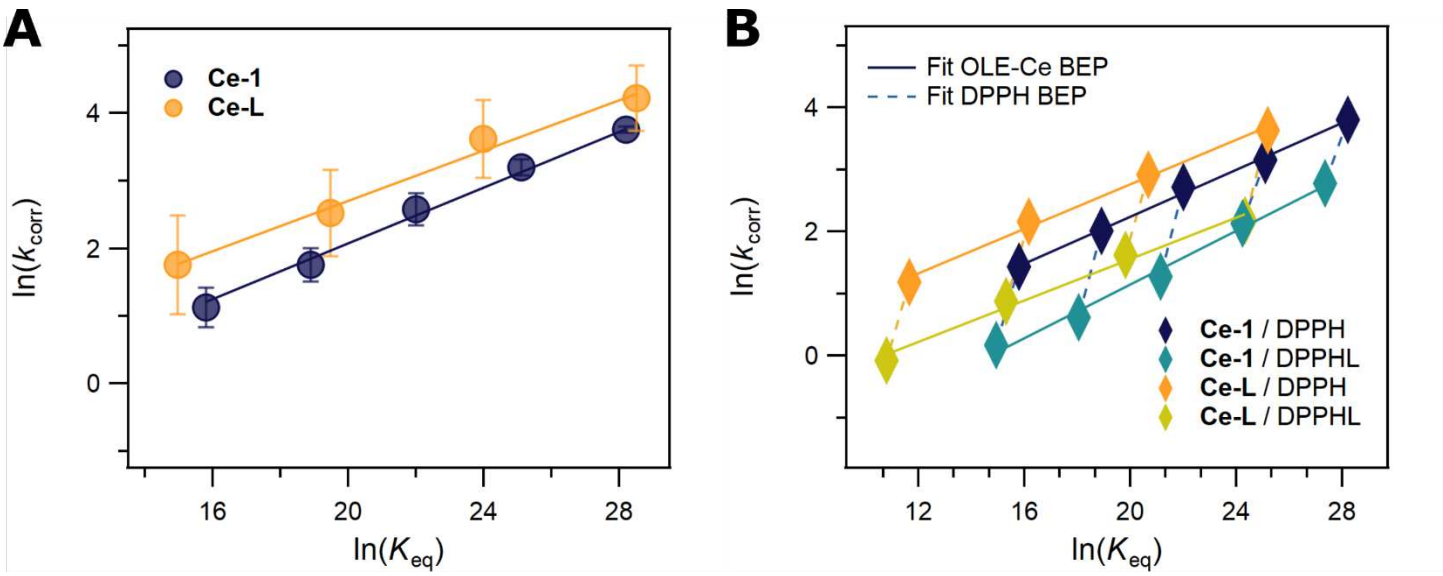

Figure 4. Dependence of the surface site adjusted reaction rate constants (ln(k_{corr})) on reaction driving force ln(K_{eq}). Values of k_{corr} are the same averages and standard deviations shown in **(A)** Figure 2A and **(B)** Figure 2B minus ln(R_{surf}). Values of ln(K_{eq}) were determined from ΔG_{rxn} = $BDFE_{Ce}$ – $BDFE_{DPPH-H}$. In (A) the slope of the **Ce-1** linear fit is 0.21 ± 0.02 and that for Ce-L is 0.19 ± 0.06, while slopes of fits in (B) are given in Table 1. Some data points in Figure 2B for **Ce-L**/DPPH are removed for simplicity.

The Ce_{active} correction does not, however, remove the gap between the DPPH and DPPHL lines (Figure 4B). In fact, the two-point dashed lines between DPPH and DPPHL data points for reactions with the same OLE-Ce stocks represent another BEP relationship. This BEP correlation is tuned by the driving force for the addition of H$^{\bullet}$ to the picrylhydrazyl, the DPPH(L)–H BDFEs, with its own slope α_{DPPH}. The fact that these lines do not overlay indicates that the slope of this BEP relationship is very different from the relationship derived from changing the $\%Ce^{3+}$ (surface H coverage) of OLE-Ce. All nine of these two-point lines have quite similar slopes, with averages of α_{DPPH} = 1.4 ± 0.2 for **Ce-1** and 1.5 ± 0.1 for **Ce-L**. Consideration of the uncertainty in ΔBDFE between DPPH and DPPHL (0.5 ± 0.2 kcal mol^{-1}) does not lower the measured to slopes below 1.2 for either **Ce-1** or **Ce-L**.

II. Nature of the Reaction Mechanism

For the data shown in Figure 4 to be assigned as traditional BEP relationships, the driving force should describe the free energy of the rate-determining step. As described above, BEP relationships relate the thermodynamic and kinetic barriers for a *single* mechanistic step. In this case the mechanism could be one step if it is hydrogen atom transfer (HAT, or concerted proton-electron transfer (CPET)), as has been discussed for other metal oxide nanoparticle systems.[57-59] If the mechanism is HAT/CPET, the slopes of the lines in Figure 4 can properly be described as Brønsted alpha's (α) relating the rate constants with the CeO–H BDFEs.

Our data do not, however, rule out mechanisms other than HAT/CPET. The overall reaction could instead involve a stepwise process, such as electron transfer (ET) followed by proton transfer (PT), inner-sphere ET involving binding of a DPPH to a surface cerium ion followed by PT and DPPH-H dissociation, the involvement of ligands, or other paths. Addition of excess oleic acid, triphenyl phosphine oxide, and DPPH-H all inhibit the reaction to a moderate extent (Figure S9B). This could suggest that dissociation of oleic acid or DPPH-H is involved in the reaction rate, or perhaps that added ligands make the nanoparticle surface more sterically congested, blocking reactive sites. This is a common observation for reactions of capped, colloidal nanoparticles.[60-63] Additionally, our previous study indicated that oleic acid protonates the surface Ce^{3+} to form $Ce(OLE)_3$, which would remove reactive sites and slow the kinetics of DPPH reduction.[45] In either case, reaction inhibition by oleic acid argues against the acid acting as a proton donor in the formation of DPPH-H. Inhibition by DPPH-H may play a role in the non-exponential character of the kinetic traces. Oleate is unlikely to be involved in the mechanism, as the addition of even small amounts results in rapid side reactions with DPPH, DPPH-H, and DPPHL-H. The product of this incompatibility absorbs in the region of the UV-vis spectra where the reaction is monitored, so it would be noticeable if oleate were formed.

To explore the possibility of rate-determining initial outer-sphere ET, we attempted to measure the 1e^{-} reduction potentials of OLE-Ce, DPPH, and DPPHL. Efforts with OLE-Ce suspensions were unsuccessful, as no faradaic features were observed by cyclic voltammetry (CV). CV experiments with both DPPH and DPPHL showed four reversible faradaic features for each substrate in THF with 0.1 M $[Bu_4N][PF_6]$ (Figure S2). Based on prior studies in other organic solvents,[64,65] the chemically reversible couples with $E_{1/2}$ = -0.329 (DPPH) and -0.261 (DPPHL) V vs $FeCp_2^{+/0}$ are assigned as the reductions of the radicals to their hydrazyl anions. The difference in half-wave potentials between DPPH and DPPHL ($\Delta E_{1/2}$) of 68 mV, or 1.6 kcal mol^{-1}, is ca. three times the difference in PCET driving force. This is consistent with the typical observation for PCET reagents that changes in $E_{1/2}$ are larger than those in BDFEs.[66] A mechanism of rate-limiting ET would be consistent with the H/D kinetic isotope effect of 1 measured under multiple conditions. It would also provide an explanation for the large changes in rate constants for DPPH vs. DPPHL, as using $\Delta E_{1/2}$ instead of ΔBDFE would reduce α_{DPPH} by a factor of three and bring it close to the expected value of 0.5. However, kinetic runs in the presence of 0, 2.7, and 5.3 mM $NaBAr^F$ (Figure S11) did not show any effect of solution ionic strength, which would have been expected to facilitate an electron transfer to make charged products.[67] Previous studies also indicated similar timescales for reactions performed in THF and toluene,[45] despite a factor of 3 difference in dielectric constants between the two solvents.[68] These results suggest that there is little charge character in the transition state, arguing against rate-limiting ET.

The delineation between stepwise and concerted PCET processes at material interfaces is one that is rarely made, and difficult even for the relatively well-defined reactions of these nanoparticles. While the ceria colloids used are as similar as we could make them—the same batch of material, just reduced by different amounts—our previous study did note reversible changes to the ligand shell and other features of these ceria colloids with increasing surface coverages of hydrogen atoms.[45] These properties could be relevant to the mechanism of net hydrogen transfer to DPPH. On balance, the available evidence suggests that charged species and outersphere ET are not involved in the reaction, though we cannot rule this out. We favor the concerted PCET mechanism.

III. Brønsted Slopes

With the tentative conclusion that the reactions are simple, one-step hydrogen atom transfer (HAT) reactions, the data shown in Figure 4 *are* traditional BEP relationships. This is, to the best of our knowledge, the first experimental example of a hydrogen coverage-dependent BEP relationship on a metal oxide material (to our knowledge, the first for any non-metallic material). The Brønsted α of 0.2 for CeO–H bond strength is far lower than the value of 0.5 commonly assumed for heterogeneous catalysis and electrocatalysis. This deviation from expectation is significant as $\alpha = 0.2$ means that an increase in equilibrium constant of 10^5 (ΔBDFE = 7 kcal mol^{-1}) gives only a factor of 10 increase in the rate constant, vs. a factor of 300 when $\alpha = 0.5$.

The Brønsted $\alpha = 0.2$ for variations in the CeO–H bond strength is far lower than the value of 0.5 commonly assumed for heterogeneous catalysis and electrocatalysis. This deviation from expectation is significant as $\alpha = 0.2$ means that an increase in equilibrium constant of 10^5 (ΔBDFE = 7 kcal mol^{-1}) gives only a factor of 10 increase in the rate constant, vs. a factor of 300 when $\alpha = 0.5$. The same 0.2 slope vs. BDFE(CeO–H) was obtained for two different sizes of ceria nanoparticles with two slightly different DPPH abstractors. However, comparing the rate constants for the two different H-atom abstractors gave much larger Brønsted slopes, ~1.4, for many 2-point lines (Figure 4B).

Brønsted slopes for molecular reactions have been discussed by physical-organic chemists for decades.[18-22] The simplest interpretation follows from the Hammond Postulate, that a shallow dependence of barrier on driving force indicates that the transition state is early along the reaction coordinate and a large Brønsted α indicates a late transition state. There are many exceptions to this simple picture, for instance when substituents affect transition state energies much more than the overall free energy of the rate limiting step (e.g., when the transition state is much more polar than the reactants or products). Two-dimensional More O'Ferrall–Jencks diagrams are often used to describe such situations, when the transition state is not simply an interpolation between reactants and products. Thus, the Brønsted α can indicate the position of the transition state along the reaction coordinate, but it frequently doesn't.

The Brønsted α's reported here do not fit the simple Hammond-postulate model. This model does not allow for differing α's upon alteration of reaction thermodynamics via the bond strength of CeO–H or that of the organic PCET oxidant, or for α values greater than 1. While the deviations from the simple model could be due to the reaction mechanisms being more complicated (see above), this section considers the implications if they are one-step H-atom transfer (HAT) or concerted PCET. We emphasize that the stepwise vs. concerted PCET level of mechanistic detail is almost never available for rate limiting steps in heterogeneous catalysis (or electrocatalysis). Analyses of rate-driving force relationships (e.g., in Volcano plots) typically make the joint assumptions of both concerted e^-/H^+ transfers (e.g., the Volmer reaction) and $\alpha = ½$. Our measured α's are relevant to those discussions.

There have been a number of recent reports of unusual Brønsted α values in molecular H-atom transfer (HAT) or concerted PCET reactions, with different interpretations.[48-51,69-72,76] Some have invoked Bernasconi's principle of non-perfect synchronization (first proposed in 1985).[49,69,73] One study of multi-site concerted PCET (MS-CPET) from our laboratory found, similar to the current interfacial study, very different Brønsted α's in response to changes in the $\Delta G°$ of the rate determining step in different ways.[49,72] Since PCET (and HAT) involve transfer of two particles, e^- and H^+, there have been suggestions that concerted (one-step) reactions can be asynchronous or imbalanced, such that the rates are more affected by the ET or the PT component of the reaction, not just the overall $\Delta G°_{PCET}$.[48,50,51,72,74,75] However, the transfer of an electron is fundamentally a quantum-mechanical process; the electron does not have a "position" and cannot be treated classically as in a More O'Ferrall–Jencks diagram.[72,75] Apparent imbalance cold be the result of the involvement of vibrational excited states, or by reactions across a series having variable intrinsic barriers (λ) or ground-state precursor-complex structures.[48-51,69-72] This is an active area of research for molecular systems. A 1986 study of interfacial Brønsted slopes by Conway and Wilkinson examined electrochemical proton discharge at mercury electrodes ($H^+ + e^- \rightarrow\rightarrow ½\ H_2$) and found differences between the behavior on varying the K_a of the acid ($\alpha = 0.37$ (in H_2O), 0.47 (in DMF), and 0.33 (in MeCN), and upon varying the applied potential (the Tafel slopes).[82] These α values are also relatively low. In the present system, the low α for changes in CeO–H BDFE could be influenced by DPPH diffusion through the ligand shell, though mass-transfer limitations seem unlikely in these slow reactions in low-viscosity THF solutions. The large α ~1.4 between DPPH and DPPHL could be in part due to their steric and hydrophobicity differences.

This extended discussion (in part prompted by questions from reviewers) shows the complexity of interpreting Brønsted slopes. In addition, any generalization from this first example should be made with caution. Still, the current study of ceria nanoparticle reactivity demonstrates the possibility of valuable connections between the molecular chemistry and interfacial reactivity. The ceria reactions seem to resemble multi-site PCET processes in molecular model systems, since the transferring proton comes from a surface OH group while the electron comes from a Ce^{3+} site which might not be adjacent in the metal oxide. Based on the results reported, and the molecular analogies, it seems likely to us that many solid/solution interfacial reactions will show significant deviations from the common assumption that the Brønsted α is close to 0.5 for heterogeneous catalysts and electrocatalysts as these materials have wide-ranging properties. Many catalysts are high surface area, nanoscale catalysts with distributions of active sites and varying surface environments, but unlike those studied here generally do not have capping ligands. Just within the class of binary oxides, there are great variations in surface structure, degree of hydration, electronic properties, and thermochemical properties.[77-79] Greater understanding of the issues raised in this section will enrich the use of linear free energy relationships in heterogeneous catalysis and electrocatalysis, and seems likely to open new paths to catalyst improvement.

Conclusions

Reduced cerium oxide/hydroxide nanoparticles (NPs) with oleate capping ligands, suspended in THF, are readily oxidized by the hydrazyl radicals DPPH and DPPH–L by net hydrogen atom transfer (HAT). Kinetic experiments show that the reactions are faster with more reduced NPs, which have previously been shown to have higher hydrogen surface coverages and lower surface CeO–H bond dissociation free energies (BDFEs). The natural log of the hydrogen transfer rate constants, ln(k), correlate linearly with the natural log of the equilibrium constants, ln(K_{eq}), over a range of NP redox levels (%Ce from 33.5% - 73.5%). This corresponds to a variation of reaction driving forces ($\Delta\Delta G°_{HAT}$) as much as 10 kcal mol. The ln(k)/ln(K_{eq}) linear relationships thus follow the Brønsted-Evans-Polanyi (BEP) relation. To our knowledge, this is the first experimental report of how the hydrogen adsorption isotherm of a material alters the kinetics of its reactivity at the solid/solution interface. These data and the result of a low Brønsted α of 0.2 therefore serve as important benchmarks for future theory studies, and suggest that variations in coverage-dependent BEP relationships across different materials may complicate many common analyses of (electro)catalyst performance.

The experiments show only a shallow dependence of rate constants on driving force: the Brønsted slope $\alpha = 0.2$ over a change of K_{eq} of 10^7 that only changes k by a factor of 25. This value of α is much smaller than typical values for HAT reactions which are close to 0.5. In addition, varying the free energy of reactions through changes in the H-atom affinity of the DPPH abstractor has a much more dramatic effect on the rate constants ($\alpha > 1$), which may suggest imbalanced e^-/H^+ transfer. These results have implications for 'volcano plot' or similar analyses of reaction kinetics at surfaces, which often use a single thermochemical descriptor for a surface, and often take $\alpha \cong 0.5$. These analyses typically assume constant surface coverage, or that coverage effects are small in magnitude or similar across all materials, so that they can be ignored. However, the chemistry of nanoceria shows that the surface coverage can significantly shift net hydrogen atom transfer kinetics and thermodynamics.

Our finding that large shifts in CeO–H BDFEs only modestly affect the rate constants for of net hydrogen transfer may provide insight into the application of ceria as a catalyst support. In this capacity, nanoceria acts as either a thermodynamic source or sink of redox equivalents for many different processes.[42,52,80,81] Our previous study posited that the wide range of CeO–H BDFEs may enable the material to facilitate a wide range of reactions.[45] The shallow BEP relationship found here takes that hypothesis one step further by demonstrating that over the wide range of CeO–H BDFEs rates of net hydrogen transfer change far less than would be expected. This could be an advantageous property for a non-innocent support which must function well across a variety of reaction conditions and driving forces.[42,52] As a result, we once again posit that these thermodynamic and kinetic properties help to provide a fundamental basis for why cerium oxide is such an exceptional catalyst support.

ASSOCIATED CONTENT

Supporting Information. A pdf file including general experimental considerations (materials, syntheses, and instrumentation), experimental kinetic procedures, properties of DPPH and DPPH-L, and additional data (mostly kinetic data) in Figures and Tables. The Supporting Information is available free of charge on the ACS Publications website.

AUTHOR INFORMATION

Corresponding Author

James M. Mayer, − Department of Chemistry, Yale University, New Haven, Connecticut 06520-8107, United States; orcid.org/0000-0002-3943-5250; Email: james.mayer@yale.edu

Rishi G. Agarwal − Department of Chemistry, Yale University; orcid.org/0000-0002-5133-0136,

Present Addresses

R.G.A.: Department of Chemistry, Stanford University, co2rishi@stanford.edu

Author Contributions

The conception and experimental studies were done by R.G.A., in consultation with J.M.M. Both of the authors actively participated in manuscript preparation and editing.

Funding Sources

No competing financial interests have been declared.

We are grateful to the National Science Foundation for support under CHE-1904813. RGA was also supported by a National Science Foundation Graduate Research Fellowship.

ACKNOWLEDGMENT

We acknowledge helpful conversations on experiment design with Prof. Anna Brezny, Dr. Brian Koronkiewicz, and Dr. Soyoung Kim. R.G.A. acknowledges support from a National Science Foundation Graduate Research Fellowship. J.M.M. acknowledge support from National Science Foundation grant CHE-1904813.

References

1. Nørskov, J. K.; Bligaard, T.; Logadottir, A.; Kitchin, J. R.; Chen, J. G.; Pandelov, S.; Stimming, U., Trends in the Exchange Current for Hydrogen Evolution. *J. Electrochem. Soc.* **2005,** *152* (3), J23-J26.
2. Schmickler, W.; Trasatti, S., Comment on "Trends in the Exchange Current for Hydrogen Evolution" [J. Electrochem. Soc., 152, J23 (2005)]. *J. Electrochem. Soc.* **2006,** *153* (12), L31-L32.
3. Quaino, P.; Juarez, F.; Santos, E.; Schmickler, W., Volcano plots in hydrogen electrocatalysis - uses and abuses. *Beilstein. J. Nanotechnol.* **2014,** *5*, 846-54.
4. Seh, Z. W.; Kibsgaard, J.; Dickens, C. F.; Chorkendorff, I.; Norskov, J. K.; Jaramillo, T. F., Combining theory and experiment in electrocatalysis: Insights into materials design. *Science* **2017,** *355* (6321), 146.
5. Bligaard, T.; Nørskov, J. K.; Dahl, S.; Matthiesen, J.; Christensen, C. H.; Sehested, J., The Brønsted–Evans–Polanyi relation and the volcano curve in heterogeneous catalysis. *J. Catal.* **2004,** *224* (1), 206-217.
6. Koper, M. T. M., Thermodynamic theory of multi-electron transfer reactions: Implications for electrocatalysis. *J. Electroanal. Chem.* **2011,** *660* (2), 254-260.
7. Cheng, J.; Hu, P.; Ellis, P.; French, S.; Kelly, G.; Lok, C. M., Brønsted−Evans−Polanyi Relation of Multistep Reactions and Volcano Curve in Heterogeneous Catalysis. *J. Phys. Chem. C* **2008,** *112* (5), 1308-1311.
8. Exner, K. S.; Over, H., Kinetics of Electrocatalytic Reactions from First-Principles: A Critical Comparison with the Ab Initio Thermodynamics Approach. *Acc. Chem. Res.* **2017,** *50* (5), 1240-1247.
9. Lindgren, P.; Kastlunger, G.; Peterson, A. A., A Challenge to the G ∼ 0 Interpretation of Hydrogen Evolution. *ACS Catal.* **2020,** *10* (1), 121-128.
10. Whittaker, T.; Kumar, K. B. S.; Peterson, C.; Pollock, M. N.; Grabow, L. C.; Chandler, B. D., H_2 Oxidation over Supported Au Nanoparticle Catalysts: Evidence for Heterolytic H_2 Activation at the Metal–Support Interface. *J. Am. Chem. Soc.* **2018,** *140* (48), 16469-16487.
11. Pérez-Ramírez, J.; López, N., Strategies to break linear scaling relationships. *Nat. Catal.* **2019,** *2* (11), 971-976.
12. Darby, M. T.; Stamatakis, M.; Michaelides, A.; Sykes, E. C. H., Lonely Atoms with Special Gifts: Breaking Linear Scaling Relationships in Heterogeneous Catalysis with Single-Atom Alloys. *J. Phys. Chem. Lett.* **2018,** *9* (18), 5636-5646.
13. Barteau, M. A., Linear free energy relationships for C_1-oxygenate decomposition on transition metal surfaces. *Catal. Lett.* **1991,** *8* (2), 175-183.
14. Akhade, S. A.; Nidzyn, R. M.; Rostamikia, G.; Janik, M. J., Using Brønsted-Evans-Polanyi relations to predict electrode potential-dependent activation energies. *Catal. Today* **2018,** *312*, 82-91.
15. van Santen, R. A.; Neurock, M.; Shetty, S. G., Reactivity Theory of Transition-Metal Surfaces: A Brønsted−Evans−Polanyi Linear Activation Energy−Free-Energy Analysis. *Chem. Rev.* **2010,** *110* (4), 2005-2048.
16. Panov, G. I.; Parfenov, M. V.; Parmon, V. N., The Brønsted−Evans−Polanyi Correlations in Oxidation Catalysis. *Catalysis Reviews* **2015,** *57* (4), 436-477.
17. Viñes, F.; Vojvodic, A.; Abild-Pedersen, F.; Illas, F., Brønsted–Evans–Polanyi Relationship for Transition Metal Carbide and Transition Metal Oxide Surfaces. *J. Phys. Chem. C* **2013,** *117* (8), 4168-4171.
18. Jencks, W. P., A primer for the Bema Hapothle. An empirical approach to the characterization of changing transition-state structures. *Chem. Rev.* **1985,** *85* (6), 511-527.
19. Kresge, A. J., The Brønsted relation – recent developments. *Chem. Soc. Rev.* **1973,** *2* (4), 475-503.
20. Kresge, A. J., Deviant Broensted relations. *J. Am. Chem. Soc.* **1970,** *92* (10), 3210-3211.
21. Pross, A., *Theoretical and Physical Principles of Organic Reactivity*. Wiley: 1995.
22. Lowry, T. H.; Richardson, K. S., *Mechanism and Theory in Organic Chemistry*. 3rd ed.; Pearson: 1987.
23. Evans, M. G.; Polanyi, M., Inertia and driving force of chemical reactions. *Trans. Faraday Soc.* **1938,** *34*, 11-24.
24. Brönsted, J. N.; Pedersen, K., Die katalytische Zersetzung des Nitramids und ihre physikalisch-chemische Bedeutung. *Z. Phys. Chem.* **1924,** *108U* (1), 185-235.
25. Baran, J. D.; Grönbeck, H.; Hellman, A., Analysis of Porphyrines as Catalysts for Electrochemical Reduction of O_2 and Oxidation of H_2O. *J. Am. Chem. Soc.* **2014,** *136* (4), 1320-1326.
26. Wang, S.; Temel, B.; Shen, J.; Jones, G.; Grabow, L. C.; Studt, F.; Bligaard, T.; Abild-Pedersen, F.; Christensen, C. H.; Nørskov, J. K., Universal Brønsted-Evans-Polanyi Relations for C–C, C–O, C–N, N–O, N–N, and O–O Dissociation Reactions. *Catal. Lett.* **2011,** *141* (3), 370-373.
27. Wang, Y.; Montoya, J. H.; Tsai, C.; Ahlquist, M. S. G.; Nørskov, J. K.; Studt, F., Scaling Relationships for Binding Energies of Transition Metal Complexes. *Catal. Lett.* **2016,** *146* (2), 304-308.
28. Campbell, C. T., The Degree of Rate Control: A Powerful Tool for Catalysis Research. *ACS Catal.* **2017,** *7* (4), 2770-2779.
29. Campbell, C. T., Future Directions and Industrial Perspectives Micro- and macro-kinetics: Their relationship in heterogeneous catalysis. *Top. Catal.* **1994,** *1* (3), 353-366.

30. Cortright, R. D.; Dumesic, J. A., Kinetics of heterogeneous catalytic reactions: Analysis of reaction schemes. In *Advances in Catalysis*, Academic Press: 2001; Vol. 46, pp 161-264.
31. Motagamwala, A. H.; Dumesic, J. A., Microkinetic Modeling: A Tool for Rational Catalyst Design. *Chem. Rev.* **2021,** *121* (2), 1049-1076.
32. Stoltze, P., Microkinetic simulation of catalytic reactions. *Prog. Surf. Sci.* **2000,** *65* (3), 65-150.
33. Parsons, R., The rate of electrolytic hydrogen evolution and the heat of adsorption of hydrogen. *Trans. Faraday Soc.* **1958,** *54*, 1053-1063.
34. Thomas, J. G. N., Kinetics of electrolytic hydrogen evolution and the adsorption of hydrogen by metals. *Trans. Faraday Soc.* **1961,** *57*, 1603-1611.
35. Conway, B. E.; Gileadi, E., Kinetic Theory of Pseudo-Capacitance and Electrode Reactions at Appreciable Surface Coverage. *Trans. Faraday Soc.* **1962,** *58*, 2493-2509.
36. Campbell, C. T.; Sellers, J. R. V., Enthalpies and Entropies of Adsorption on Well-Defined Oxide Surfaces: Experimental Measurements. *Chem. Rev.* **2013,** *113* (6), 4106-4135.
37. Strmcnik, D.; Tripkovic, D.; van der Vliet, D.; Stamenkovic, V.; Marković, N. M., Adsorption of hydrogen on Pt(111) and Pt(100) surfaces and its role in the HOR. *Electrochem. Commun.* **2008,** *10* (10), 1602-1605.
38. Skúlason, E.; Tripkovic, V.; Björketun, M. E.; Gudmundsdóttir, S.; Karlberg, G.; Rossmeisl, J.; Bligaard, T.; Jónsson, H.; Nørskov, J. K., Modeling the Electrochemical Hydrogen Oxidation and Evolution Reactions on the Basis of Density Functional Theory Calculations. *J. Phys. Chem. C* **2010,** *114* (42), 18182-18197.
39. Bard, A. J.; Faulkner, L. R., *Electrochemical Methods: Fundamentals and Applications*. John Wiley & Sons: NY, 2nd edition, 2001, p. 591 for the CV of an ideal Nernstian reaction following a Langmuir isotherm.
40. German, E. D.; Abir, H.; Sheintuch, M., A Tunnel Model for Activated Hydrogen Dissociation on Metal Surfaces. *J. Phys. Chem. C* **2013,** *117* (15), 7475-7486.
41. Kibsgaard, J.; Tsai, C.; Chan, K.; Benck, J. D.; Nørskov, J. K.; Abild-Pedersen, F.; Jaramillo, T. F., Designing an improved transition metal phosphide catalyst for hydrogen evolution using experimental and theoretical trends. *Energy Environ. Sci.* **2015,** *8* (10), 3022-3029.
42. Ganduglia-Pirovano, M. V., The non-innocent role of cerium oxide in heterogeneous catalysis: A theoretical perspective. *Catal. Today* **2015,** *253*, 20-32.
43. Campbell, C. T.; Sellers, J. R., Enthalpies and entropies of adsorption on well-defined oxide surfaces: experimental measurements. *Chem. Rev.* **2013,** *113* (6), 4106-35.
44. Kunimatsu, K.; Senzaki, T.; Samjeské, G.; Tsushima, M.; Osawa, M., Hydrogen adsorption and hydrogen evolution reaction on a polycrystalline Pt electrode studied by surface-enhanced infrared absorption spectroscopy. *Electrochim. Acta* **2007,** *52* (18), 5715-5724.
45. Agarwal, R. G.; Kim, H. J.; Mayer, J. M., Nanoparticle O–H Bond Dissociation Free Energies from Equilibrium Measurements of Cerium Oxide Colloids. *J. Am. Chem. Soc.* **2021,** *143* (7), 2896-2907.
46. Warburton, R. E.; Mayer, J. M.; Hammes-Schiffer, S., Proton-Coupled Defects Impact O–H Bond Dissociation Free Energies on Metal Oxide Surfaces. *J. Phys. Chem. Lett.* **2021,** *12* (40), 9761-9767.
47. Delley, M. F.; Wu, Z.; Mundy, M. E.; Ung, D.; Cossairt, B. M.; Wang, H.; Mayer, J. M., Hydrogen on Cobalt Phosphide. *J. Am. Chem. Soc.* **2019,** *141* (38), 15390-15402.
48. Bím, D.; Maldonado-Domínguez, M.; Rulíšek, L.; Srnec, M., Beyond the classical thermodynamic contributions to hydrogen atom abstraction reactivity. *Proc. Natl. Acad. Sci. U.S.A.* **2018,** *115* (44), E10287-E10294.
49. Darcy, J. W.; Kolmar, S. S.; Mayer, J. M., Transition State Asymmetry in C–H Bond Cleavage by Proton-Coupled Electron Transfer. *J. Am. Chem. Soc.* **2019,** *141* (27), 10777-10787.
50. Barman, S. K.; Yang, M.-Y.; Parsell, T. H.; Green, M. T.; Borovik, A. S., Semiempirical method for examining asynchronicity in metal–oxido-mediated C–H bond activation. *Proc. Natl. Acad. Sci. U.S.A.* **2021,** *118* (36), e2108648118.
51. Goetz, M. K.; Anderson, J. S., Experimental Evidence for pK_a-Driven Asynchronicity in C–H Activation by a Terminal Co(III)–Oxo Complex. *J. Am. Chem. Soc.* **2019,** *141* (9), 4051-4062.
52. Sayle, T. X. T.; Caddeo, F.; Zhang, X.; Sakthivel, T.; Das, S.; Seal, S.; Ptasinska, S.; Sayle, D. C., Structure–Activity Map of Ceria Nanoparticles, Nanocubes, and Mesoporous Architectures. *Chem. Mater.* **2016,** *28* (20), 7287-7295.
53. Wise, C. F.; Agarwal, R. G.; Mayer, J. M., Determining Proton-Coupled Standard Potentials and X–H Bond Dissociation Free Energies in Nonaqueous Solvents Using Open-Circuit Potential Measurements. *J. Am. Chem. Soc.* **2020,** *142* (24), 10681-10691.
54. Burés, J., Variable Time Normalization Analysis: General Graphical Elucidation of Reaction Orders from Concentration Profiles. *Angew. Chem. Int. Ed.* **2016,** *55* (52), 16084-16087.
55. Hayoun, R.; Whitaker, K. M.; Gamelin, D. R.; Mayer, J. M., Electron Transfer Between Colloidal ZnO Nanocrystals. *J. Am. Chem. Soc.* **2011,** *133* (12), 4228-4231.

56. Castillo-Lora, J.; Mitsuhashi, R.; Mayer, J. M., Revealing the Relative Electronic Landscape of Colloidal ZnO and TiO2 Nanoparticles via Equilibration Studies. *J. Phys. Chem. C* **2019,** *123* (16), 10262-10271.
57. Schrauben Joel, N.; Hayoun, R.; Valdez Carolyn, N.; Braten, M.; Fridley, L.; Mayer James, M., Titanium and Zinc Oxide Nanoparticles Are Proton-Coupled Electron Transfer Agents. *Science* **2012,** *336* (6086), 1298-1301.
58. Braten, M. N.; Gamelin, D. R.; Mayer, J. M., Reaction Dynamics of Proton-Coupled Electron Transfer from Reduced ZnO Nanocrystals. *ACS Nano* **2015,** *9* (10), 10258-10267.
59. Volpato, G. A.; Bonetto, A.; Marcomini, A.; Mialane, P.; Bonchio, M.; Natali, M.; Sartorel, A., Proton coupled electron transfer from Co_3O_4 nanoparticles to photogenerated $Ru(bpy)_3^{3+}$: base catalysis and buffer effect. *Sustainable Energy & Fuels* **2018,** *2* (9), 1951-1956.
60. Ung, D.; Cossairt, B. M., Effect of Surface Ligands on CoP for the Hydrogen Evolution Reaction. *ACS Appl. Energy Mater.* **2019,** *2* (3), 1642-1645.
61. Kuhn, J. N.; Tsung, C.-K.; Huang, W.; Somorjai, G. A., Effect of organic capping layers over monodisperse platinum nanoparticles upon activity for ethylene hydrogenation and carbon monoxide oxidation. *J. Catal.* **2009,** *265* (2), 209-215.
62. Li, D.; Wang, C.; Tripkovic, D.; Sun, S.; Markovic, N. M.; Stamenkovic, V. R., Surfactant Removal for Colloidal Nanoparticles from Solution Synthesis: The Effect on Catalytic Performance. *ACS Catal.* **2012,** *2* (7), 1358-1362.
63. De Roo, J.; Van Driessche, I.; Martins, J. C.; Hens, Z., Colloidal metal oxide nanocrystal catalysis by sustained chemically driven ligand displacement. *Nature Materials* **2016,** *15* (5), 517-521.
64. Solon, E.; Bard, A. J., The Electrochemistry of Diphenylpicrylhydrazyl. *J. Am. Chem. Soc.* **1964,** *86* (10), 1926-1928.
65. Solon, E.; Bard, A. J., Coulometric Study of the Reaction of Diphenylpicrylhydrazyl and Bromide Ion[1]. *J. Phys. Chem.* **1964,** *68* (5), 1144-1147.
66. Agarwal, R. G.; Coste, S. C.; Groff, B. D.; Heuer, A. M.; Noh, H.; Parada, G. A.; Wise, C. F.; Nichols, E. M.; Warren, J. J.; Mayer, J. M., Free Energies of Proton-Coupled Electron Transfer Reagents and Their Applications. *Chem. Rev.* **2022,** *122* (1), 1-49.
67. Valdez, C. N.; Delley, M. F.; Mayer, J. M., Cation Effects on the Reduction of Colloidal ZnO Nanocrystals. *J. Am. Chem. Soc.* **2018,** *140* (28), 8924-8933.
68. Lide, D. R., *CRC Handbook of Chemistry and Physics*. 90 ed.; CRC Press: Boca Raton, FL, 2009.
69. Salamone, M.; Galeotti, M.; Romero-Montalvo, E.; van Santen, J. A.; Groff, B. D.; Mayer, J. M.; DiLabio, G. A.; Bietti, M., Bimodal Evans–Polanyi Relationships in Hydrogen Atom Transfer from $C(sp^3)$–H Bonds to the Cumyloxyl Radical. A Combined Time-Resolved Kinetic and Computational Study. *J. Am. Chem. Soc.* **2021,** *143* (30), 11759-11776.
70. Sayfutyarova, E. R.; Lam, Y.-C.; Hammes-Schiffer, S., Strategies for Enhancing the Rate Constant of C–H Bond Cleavage by Concerted Proton-Coupled Electron Transfer. *J. Am. Chem. Soc.* **2019,** *141* (38), 15183-15189.
71. Sayfutyarova, E. R.; Goldsmith, Z. K.; Hammes-Schiffer, S., Theoretical Study of C–H Bond Cleavage via Concerted Proton-Coupled Electron Transfer in Fluorenyl-Benzoates. *J. Am. Chem. Soc.* **2018,** *140* (46), 15641-15645.
72. Coste, S. C.; Brezny, A. C.; Koronkiewicz, B.; Mayer, J. M., C–H oxidation in fluorenyl benzoates does not proceed through a stepwise pathway: revisiting asynchronous proton-coupled electron transfer. *Chem. Sci.* **2021,** *12* (39), 13127-13136.
73. Bernasconi, C. F., The principle of nonperfect synchronization: recent developments. In *Adv. Phys. Org. Chem.*, Richard, J. P., Ed. Academic Press: 2010; Vol. 44, pp 223-324.
74. Schneider, J. E.; Goetz, M. K.; Anderson, J. S., Statistical analysis of C–H activation by oxo complexes supports diverse thermodynamic control over reactivity. *Chem. Sci.* **2021,** *12* (11), 4173-4183.
75. Costentin, C.; Savéant, J.-M., Hydrogen and proton exchange at carbon. Imbalanced transition state and mechanism crossover. *Chem. Sci.* **2020,** *11* (4), 1006-1010.
76. Qiu, G.; Knowles, R. R., Rate–Driving Force Relationships in the Multisite Proton-Coupled Electron Transfer Activation of Ketones. *J. Am. Chem. Soc.* **2019,** *141* (6), 2721-2730.
77. Finklea, H. O., *Semiconductor Electrodes*. El Sevier: Amsterdam, 1988; p 520.
78. Fleischmann, S.; Mitchell, J. B.; Wang, R.; Zhan, C.; Jiang, D.-e.; Presser, V.; Augustyn, V., Pseudocapacitance: From Fundamental Understanding to High Power Energy Storage Materials. *Chem. Rev.* **2020,** *120* (14), 6738-6782.
79. Fierro, J. L. G., *Metal Oxides: Chemistry and Applications*. CRC Press: Boca Raton, 2005; p 808.
80. Vilé, G.; Bridier, B.; Wichert, J.; Pérez-Ramírez, J., Ceria in Hydrogenation Catalysis: High Selectivity in the Conversion of Alkynes to Olefins. *Angew. Chem. Int. Ed.* **2012,** *51* (34), 8620-8623.
81. Luo, M.; Wang, Z.; Li, Y. C.; Li, J.; Li, F.; Lum, Y.; Nam, D.-H.; Chen, B.; Wicks, J.; Xu, A.; Zhuang, T.; Leow, W. R.; Wang, X.; Dinh, C.-T.; Wang, Y.; Wang, Y.; Sinton, D.; Sargent, E. H., Hydroxide promotes carbon dioxide electroreduction to ethanol on copper via tuning of adsorbed hydrogen. *Nature Communications* **2019,** *10* (1), 5814.
82. Conway, B. E.; Wilkinson, D. P. Brønsted Relationships for Heterogeneous Proton Transfer at Electrode Interfaces *J. Chem. Soc., Faraday Trans. I* **1988**, *84* (10), 3389-3400.

TOC Graphic